XLVI CILAMCE
VITÓRIA - ES - BRAZIL - 2025
XLVI IBERO-LATIN AMERICAN CONGRESS ON COMPUTATIONAL METHODS IN ENGENEERING

Dynamic analysis of a simply supported fluid-conveying pipe with a mass attached at the middle of the span

Milton A. Oliveira[1], Reyolando M.L.R.F. Brasil[2]

[1]*Department of Mechanical Engineering, Federal University of ABC*
Av. dos Estados, 5001 - Bangu, 09280-560, Santo André/ S. Paulo, Brazil
milton.aparicio@ufabc.edu.br
[2]*Department of Mechanical Engineering, Federal University of ABC*
Av. dos Estados, 5001 - Bangu, 09280-560, Santo André/ S. Paulo, Brazil
reyolando.brasil@ufabc.edu.br

Abstract. In this paper, the planar dynamics of a fluid-conveying pipe, simply supported, with a mass attached at the middle span, are analyzed. Primarily, as external forces, a pulse load applied at the middle point, and the self-weight of the pipe-fluid system, were considered. For such loads, the dynamic behaviour was analyzed for different flow velocities. Additionally, to the current external applied forces, a gravitational force has been considered, because of the attached mass at the mid span. The pipe was considered an Euler-Bernoulli beam having a non-negligible flexural rigidity. Only transversal and angular displacements related to the undeformed pipe axis were considered. We assume an incompressible fluid and an elastic pipe material. The equation of motion for the model is obtained using Hamilton's variational principle. The direct integration of the dynamic equations was solved by the Galerkin's method. Numerical analyzes and simulations were performed using a code developed in Matlab. This paper demonstrated that, in the presence of the attached mass, for different flow velocities, the system frequencies decrease with time, for increasing flow velocities, approaching to zero at the theoretical critical velocity.

Keywords: Dynamic systems, Fluid-structure interactions

1 Introduction

Rigid pipes are of fundamental importance in riser systems for operations in oil, and gas industry, and also in deep and ultra-deep water operations. In such systems, the internal fluid is composed of a mixture of oil, gas, and water, flowing under different conditions of pressure, and temperature, known as slug flow. In particular, slug flow is a frequent operational phenomenon that occurs in the offshore industry. The dynamic nature of the slug pattern induces variable forces over time, leading to structural vibrations of the riser systems. These vibrations can produce considerable deflections, and stresses, which can cause excessive bending, local buckling, or failure due to fatigue. These conditions make its mathematical modeling highly complex. The study of riser systems under dynamic loads induced by a multiphase internal flow in deep waters is recent. Particularly in the offshore oil, and gas industry, there are some papers dedicated to the analysis of internal flow-conveying risers. Some authors have analyzed the dynamic behavior of the riser systems, involving relevant issues, such as the effect of the pipe flexural stiffness, the influence of large deformations, and the influence of the pulsatile internal flow, among others. **Wu and Lou [1]** developed a mathematical model to study the simultaneous effect of the flow of internal fluid, and the flexural rigidity of the pipe, on the dynamic behavior of flexible risers. The authors concluded that the flexural stiffness had a great influence on the dynamic response of the riser, under internal flow at high velocities. **Yamamoto [2]** carried out experiments on the effect of the flow of internal fluid, on the dynamic behavior of vertical pipes. The author noted that the pipe natural frequency tends to decrease with increasing fluid flow. **Onuoha et al. [3]** considered a linear structural model with small displacements, including the effects of axial traction. They developed the governing equation and used for its numerical resolution, the technique approximated by finite differences.

2 Governing equation

A simply supported pipe is considered in Fig. 1. Where $x - y$ is the Cartesian coordinate system, with the $x-$axis along the neutral line of the undeformed pipe, $y-$axis is the direction of the vertical displacements along the deformed pipe, $w(x,t)$ is the vertical displacement of the deformed pipe at $x-$coordinate, at time, t. $\theta(x,t) = \frac{\partial w(x,t)}{\partial x}$ is the slope of deformed pipe, at $x-$coordinate, at time, t, relative to the undeformed pipe, L is the free span of the pipe, D_i, and D_e are respectively the internal and external diameters of the pipe, **U** is the constant velocity vector of the fluid with direction normal to the cross section at $x-$coordinate of the deformed pipe, and m is the mass attached at the middle span of the pipe. The basic hypotheses for the system are: a) Flow of incompressible fluid only in the $x - y$ plane, with a constant velocity U [m/s]. b) The length of the pipe is much larger than the internal diameter. c) The vertical deflection w, and the slope θ, are small compared with the beam length, then the small displacements and angle assumption shall be used. d) The flow of fluid is turbulent. e) Hooke's law behavior of the pipe material is assumed. f) In the horizontal direction, the displacements are neglected. g) The cross-sections of the deformed pipe remains orthogonal to the deformed axis. h) External damping is neglected.

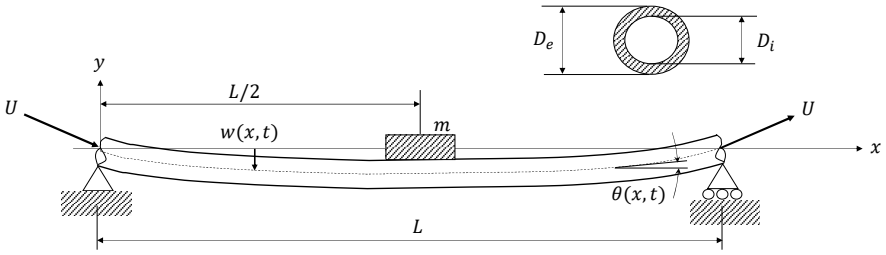


Figure 1. System scheme - Pipe with a mass attached at the middle of the free span.

2.1 Euler-Bernoulli beam model

The potential energy of a uniform beam due to bending is given by **Petyt [4]**:

$$U = \frac{1}{2}\int_0^L E\,I_z \left[\frac{\partial^2 w(x,t)}{\partial x^2}\right]^2 dx \tag{1}$$

where E is the modulus of elasticity, I_z is the moment of inertia of the cross-section about the neutral axis, $w(x,t)$ is the transverse deflection at the axial location x and time t, and L is the length of the pipe. The kinetic energy of the pipe is given by

$$T = \frac{1}{2}\int_0^L \rho_b\,A_b \left[\frac{\partial w(x,t)}{\partial t}\right]^2 dx \tag{2}$$

where ρ_b is the density of the pipe, and A_b is the cross-sectional area of the pipe. For the pipe distributed load per unit length, p_y, the force in increment, dx, is $p_y dx$. The virtual work done by the non conservative load, p_y, with a virtual displacement, $\delta w(x,t)$, is $\delta w(x,t)\; p_y dx$. Then, the virtual work for the element is therefore:

$$\delta W_{nc} = \int_0^L p_y\,\delta w(x,t) dx \tag{3}$$

The mathematical statement of Hamilton's principle is shown to be, according to **Petyt [4]**:

$$\int_{t_1}^{t_2} \left[\delta(T-U) + \delta W_{nc}\right] dt = 0 \tag{4}$$

Substituting Eq. (1), Eq. (2) and Eq. (3) into Eq. (4), and integrating by parts, gives the governing differential equation of motion for the pipe:

$$E\,I_z \frac{\partial^4 w(x,t)}{\partial x^4} + \rho_b\,A_b \frac{\partial^2 w(x,t)}{\partial t^2} = p_y \tag{5}$$

The null integrated terms left of Eq. (5), are given by:

$$\left[E\,I_z\,\frac{\partial^2 w(x,t)}{\partial x^2}\,\delta\left(\frac{\partial w}{\partial x}\right)\right]_0^L = 0, \quad \left[E\,I_z\,\frac{\partial^3 w(x,t)}{\partial x^3}\,\delta w\right]_0^L = 0 \tag{6}$$

where, according to **Timoshenko [5]** the term, $E\,I_z\,\frac{\partial^2 w(x,t)}{\partial x^2}$, represents the bending moment, and the term, $E\,I_z\,\frac{\partial^3 w(x,t)}{\partial x^3}$, represents the shear force. For Eq. (6) to be satisfied, the following pinned-pinned boundary conditions hold,

$$w(0,t) = 0, \quad E\,I_z\,\frac{\partial^2 w(0,t)}{\partial x^2} = 0 \tag{7}$$

at the left end $(x = 0)$, and

$$w(L,t) = 0, \quad E\,I_z\,\frac{\partial^2 w(L,t)}{\partial x^2} = 0 \tag{8}$$

at the right end $(x = L)$.

2.2 System fluid model

The kinetic energy for the fluid is given by

$$T_f = \frac{1}{2}\int_0^L \rho_f\,A_f\,\left(\frac{D}{D\,t}\left[w(x,t)\right]\right)^2 dx \tag{9}$$

where ρ_f is the density of the fluid and A_f the pipe internal cross-sectional area. The *material derivative* or the *convected derivative*, $D/Dt[w(x,t)]$ of the fluid, considering the flow in the x-direction, flowing with a constant velocity profile, U, inside the pipe, is given by **Blevins [6]**:

$$\frac{D}{D\,t}\left[w(x,t)\right] = \left(\frac{\partial}{\partial t} + U\,\frac{\partial}{\partial x}\right) w(x,t) \tag{10}$$

where $\frac{\partial}{\partial t}$ is the partial derivative relative to time, and $\frac{\partial}{\partial x}$ the partial derivative relative to space, since the motion is planar $(z = 0)$. Note that, it's assumed here that it does not have any flow velocity say, V_y, in y direction, which implies that there is no the term, $\frac{\partial}{\partial y}$, in Eq. (10). Then, substituting the Eq. (10) in Eq. (9) gives the kinetic energy of the fluid:

$$T_f = \frac{1}{2}\int_0^L m_f\,\left[\left(\frac{\partial}{\partial t} + U\,\frac{\partial}{\partial x}\right) w(x,t)\right]^2 dx \tag{11}$$

where, $m_f = \rho_f\,A_f$, is the fluid mass, by unit length. Developing the integrand of Eq. (11), and integrating by parts, we get the expression for the forces acting on an element of fluid, due to the induced accelerations that appears on it's motion:

$$m_f\,\left[\frac{\partial^2}{\partial t^2} w\,(x,t) + 2\,U\,\frac{\partial^2}{\partial t \partial x} w\,(x,t) + U^2\,\frac{\partial^2}{\partial x^2} w\,(x,t)\right] \tag{12}$$

where, the first term stands for the inertial force of the element of fluid. The second, and third terms represent, respectively, the Coriolis, and the centrifugal effects on the fluid motion, due to the fluid relative velocity with respect to the pipe. Adding Eq. (12) to Eq. (5), gives the fluid-pipe system governing equation as follows, according to **Blevins [6]**:

$$E\,I_z\,\frac{\partial^4 w(x,t)}{\partial x^4} + m_f\left(2\,U\,\frac{\partial^2 w(x,t)}{\partial t\,\partial x} + U^2\,\frac{\partial^2 w(x,t)}{\partial x^2}\right) + M_c\,\frac{\partial^2 w(x,t)}{\partial t^2} - p_y = 0 \tag{13}$$

Defining the quantity, $m_t = \rho_b A_b$, as linear mass of the pipe, the quantity $M_c = m_f + m_t$ is the mass of the system, per unit length. Then, the fourth term in Eq. (13) represents the system total inertia force. The external concentrated loads applied on the system are composed of a pulse load, and the weight of the mass attached. The pulse load $p_L = P(t)$, is a known time variable force, and in section 4 it is described what is the form of this force. These external concentrated loads are the components of the external force vector, $\{R^{ext}\}$, as described in section 3.1 .

3 SIMULATIONS BY FINITE ELEMENT ANALYSIS

3.1 Finite element formulation

The weak formulation is obtained by Galerkin's method applied to Eq. (13). According to **Cook [7]**, the resulting discretization in finite elements is made by considering the nodal displacement vector $\{d(t)\}^e$ for an element, e, dependent on time as:

$$\{d(t)\}^e = \lfloor u_1(t) \quad \theta_1(t) \quad u_2(t) \quad \theta_2(t) \rfloor^T \tag{14}$$

where, $u_1(t), u_2(t)$ are the nodal vertical displacements, and $\theta_1(t), \theta_2(t)$ are the nodal rotations, at nodes 1 and 2 of element, e, respectively. The externally applied loads on the element are represented by the element nodal force vector, $\{r\}^e = \lfloor V_1^e \quad M_1^e \quad V_2^e \quad M_2^e \rfloor^T$, where: V_1^e, V_2^e are the nodal shear forces, and M_1^e, M_2^e are the nodal bending moments, at nodes 1 and 2 of the element, e, respectively. The shape function matrix for a beam element is given by:

$$[N(x)]^e = \lfloor 1 - 3\,\frac{x^2}{L^2} + 2\,\frac{x^3}{L^3}, \quad x - 2\,\frac{x^2}{L} + \frac{x^3}{L^2}, \quad 3\,\frac{x^2}{L^2} - 2\,\frac{x^3}{L^3}, \quad -\frac{x^2}{L} + \frac{x^3}{L^2} \rfloor \tag{15}$$

where L is the length of the element. The transversal displacement $w(x,t)$ of the beam is approximated in FEA by the product of the shape function matrix in Eq. (15), and the nodal displacement vector in Eq. (14) as:

$$w(x,t) = [N(x)]^e \ \{d(t)\}^e \tag{16}$$

Time and space derivatives are noted, respectively, as the symbols dot, $\dot{}$, and prime, $'$, over the differentiated variables. Hence, substituting Eq. (16) into Eq. (13), gives,

$$[m]^e\{\ddot{d}(t)\} + [c]^e\{\dot{d}(t)\} + ([k]^e - [c_f]^e)\,\{d(t)\} = \{r\}^e \tag{17}$$

where the vectors $\{d(t)\}$, $\{\dot{d}(t)\}$ and $\{\ddot{d}(t)\}$ are, respectively, the nodal displacement vector, the nodal velocity vector, and the nodal acceleration vector. Furthermore, for an element, e, the matrices $[k]^e$, $[c_f]^e$, $[m]^e$, and $[c]^e$ are, respectively, the stiffness, centrifugal, mass, and dissipation matrices. Using the shape functions defined in Eq. (15), and the corresponding derivatives with respect to x, and, t, the matrices $[k]^e, [c_f]^e$, $[m]^e$, and $[c]^e$ in Eq. (17) can be determined, by direct integration. Therefore, the element stiffness, centrifugal, and mass matrices, are given, respectively, by:

$$[k]^e = E\,I_z \int_0^L [N'']^T\,[N'']dx \ = \frac{E\,I_z}{L^3} \begin{bmatrix} 12 & 6\,L & -12 & 6\,L \\ 6\,L & 4\,L^2 & -6\,L & 2\,L^2 \\ -12 & -6\,L & 12 & -6\,L \\ 6\,L & 2\,L^2 & -6\,L & 4\,L^2 \end{bmatrix} \tag{18}$$

$$[c_f]^e = U^2\,m_f \int_0^L [N']^T\,[N']dx = \frac{U^2\,m_f}{30\,L} \begin{bmatrix} 36 & 3\,L & -36 & 3\,L \\ 3\,L & 4\,L^2 & -3\,L & -L^2 \\ -36 & -3\,L & 36 & -3\,L \\ 3\,L & -L^2 & -3\,L & 4\,L^2 \end{bmatrix} \tag{19}$$

$$[m]^e = M_c \int_0^L [N]^T\,[N]dx = \frac{M_c\,L}{420} \begin{bmatrix} 156 & 22\,L & 54 & -13\,L \\ 22\,L & 4\,L^2 & 13\,L & -3\,L^2 \\ 54 & 13\,L & 156 & -22\,L \\ -13\,L & -3\,L^2 & -22\,L & 4\,L^2 \end{bmatrix} \tag{20}$$

The dissipation matrix, also named the Coriolis matrix, is given by[1]:

$$[c]^e = 2\,U\,m_f \int_0^L [N]^T\,[N']dx = \frac{U\,m_f}{30} \begin{bmatrix} -30 & -6\,L & -30 & 6\,L \\ 6\,L & 0 & -6\,L & L^2 \\ 30 & 6\,L & 30 & -6\,L \\ -6\,L & -L^2 & 6\,L & 0 \end{bmatrix} \tag{21}$$

[1]It can be noted that the matrices $[k]^e$, $[c_f]^e$, and $[m]^e$ are symmetric matrices, against the Coriolis matrix, $[c]^e$, which *is not*.

Afterward, the stiffness, mass, and dissipation matrices for the finite element, e, have been determined, the global matrices are assembled according to the respective element matrices, considering the number of finite elements, N, in which the system was discretized for analysis by FEM. This leads to the dynamic equation of the system, given by:

$$[M]\{\ddot{D}\} + [C]\{\dot{D}\} + [K]\{D\} = \{R^{ext}\} \tag{22}$$

where, the matrices, $[M]$, $[C]$, and $[K]$, are respectively, the global mass matrix, the global dissipation matrix, and the global stiffness matrix of the system. The vectors, $\{D\}$, $\{\dot{D}\}$, and $\{\ddot{D}\}$ are, respectively, the global nodal displacement, the global nodal velocity, and the global nodal acceleration vectors of the system. The vector, $\{R^{ext}\}$, is the global nodal external force vector applied to the system.

4 Results

Crude oil flow in pipelines are considered in this section. The design range of oil industry guidelines typically set flow velocities between 1,0 $\mathrm{m/s}$ and 3,0 $\mathrm{m/s}$ for crude oil in large onshore pipelines. A crude oil flow rate of 9172 $\mathrm{m^3/d}$ (0,1065 $\mathrm{m^3/s}$) flowing in a nominal OD 0,400 m piping (ID 0,406 m), wall thickness: $12.7\,\mathrm{mm}$, was considered. Therefore, the flow velocity considered is approximately 0,82 $\mathrm{m/s}$. This value ($\approx$ 0,8 $\mathrm{m/s}$) is close to the recommended lower limit, minimizing deposits, but still effective for long-distance transport[2].

4.1 Natural frequencies of the system

We adopt, a simply supported pipe with span, $\mathrm{L} = 10.97\,\mathrm{m}$ (36 ft). For the pipe with Young's modulus of $E = 207 \times 10^9\,\mathrm{N/m^2}$, linear mass of $\mathrm{m}_{pipe} = 123.16\,\mathrm{kg/m}$, and linear weight of $\mathrm{p}_{pipe} = 1208.20\,\mathrm{N/m}$. The internal fluid is crude oil, where: linear mass of $\mathrm{M}_{fluid} = 110.04\,\mathrm{kg/m}$, and linear weight of $\mathrm{p}_{fluid} = 1079.50\,\mathrm{N/m}$. Firstly, we consider empty pipe. According to **Timoshenko [5]**, the theoretical maximum deflection in the middle of the span, for simply supported pipe, is given by: $\mathrm{f}_{max} = \frac{5\,\mathrm{p}_{pipe}\,L^4}{384\,EI}$. With data, this ensures maximum deflection in the middle of the span of $0.0033\,\mathrm{m} < 0.006\,\mathrm{m}$, which is in accordance with N-57, by **Petrobras [8]**. Initially, considering only one finite element, i.e., $N = 1$, for pinned-pinned boundary condition, with empty pipe. Then $[C] = 0$. The mass matrix is, $[M] = \frac{\mathrm{m}_{pipe}\,L}{420}\begin{bmatrix} 4\,L^2 & -3\,L^2 \\ -3\,L^2 & 4\,L^2 \end{bmatrix} = 10^3 \times \begin{bmatrix} 1.55 & -1.16 \\ -1.16 & 1.55 \end{bmatrix}$. The stiffness matrix is, $[K] = \frac{E\,I_z}{L^3}\begin{bmatrix} 4\,L^2 & 2\,L^2 \\ 2\,L^2 & 4\,L^2 \end{bmatrix} = 10^5 \times \begin{bmatrix} 276.5 & 138.3 \\ 138.3 & 276.5 \end{bmatrix}$. The minimum natural frequency for empty pipe is given by the Hermitian matrix, as follows:

$[H] = \begin{bmatrix} -[M]^{-1}[C] & -[M]^{-1}[K] \\ Id & 0 \end{bmatrix}$ where, Id and 0, are the identity and zero matrices, respectively. Both matrices have the same dimensions as $[M]$, and $[K]$ matrices. With data, we find: $\omega_{min} = 71.38\,\mathrm{rad/s}$. According to **Grant [9]**, the fundamental frequency is: $\omega_1 = (\pi/L)^2\sqrt{EI/\mathrm{m}_{pipe}} = 64.32\,\mathrm{rad/s}$. The observed difference of, $71.38/64.32 = 1.11$, or, 11%, in the minimum frequencies of the system is because of the number of finite elements initially adopted $N = 1$. As the number of elements increases, the calculated value for the fundamental frequency of the system will approach the theoretical value. Indeed, for only $N = 2$ elements, the calculated natural frequency is $64.57\,\mathrm{rad/s}$, or, 0.40% of difference relative to the theoretical value. For, $N = 10$ elements, the calculated natural frequency is $64.31\,\mathrm{rad/s}$. Secondly, we consider full pipe for different flow velocities, for system discretized with, $N = 10$ elements. Table 1 shows that as the oil flow velocity in the pipe increases, the natural frequency of the system decreases. However, the system remains stable, with only small variations in the natural frequencies. Notice in Tab. 1, two flow velocity ranges. The first, ranging from 0 to 3 m/s, is within the operating limit range, as described above. The second range, from 4 to 6 m/s, is theoretical, only for the purpose of verifying the stability of the system. Finally, we add a mass of $100\,\mathrm{kg}$, in the middle span of the pipe. Then, we repeat the same sample for the flow velocities and the corresponding frequencies of the system are displayed at third column.

In Fig. (2), it can be seen that the response of the natural frequencies of the system, with increasing fluid flow velocity, without the addition of the central mass. Notice that, as the fluid flow velocity increases, the frequency of the system decreases. The flow velocity values were extrapolated outside the aforementioned operating range, in order to find the critical flow velocity of the system, at which the frequency is zero. This is the limit where the system exhibits static instability, also known as divergence instability. For high fluid flow velocities, the dynamic

[2]Notice that the piping does not have any thermal insulation.

Table 1. System natural frequencies for full pipe with added mass

Flow velocity [m/s]	Frequency Value [rad/s]	With added mass of 100 [kg]
0	46.7431	45.0155
0.8	46.7428	45.0153
1.0	46.7426	45.0151
1.5	46.7421	45.0146
2.0	46.7413	45.0138
2.5	46.7403	45.0128
3.0	46.7390	45.0117
4.0	46.7359	45.0086
5.0	46.7318	45.0047
6.0	46.7268	45.0000

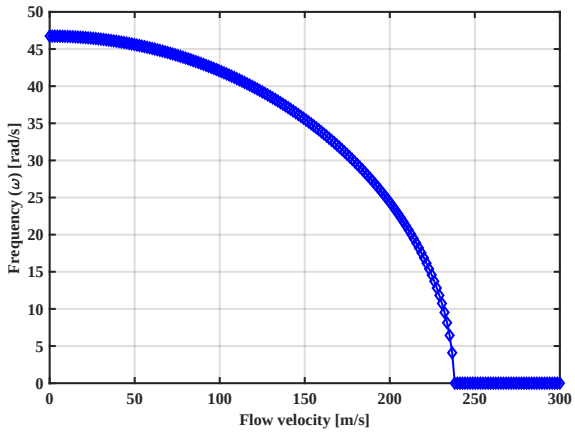


Figure 2. Flow velocity X Frequency.

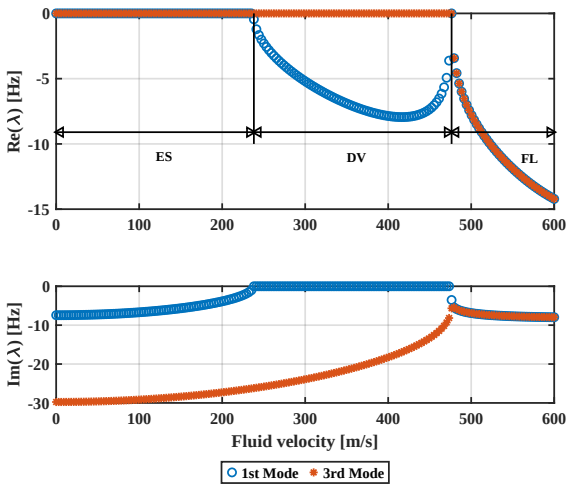


Figure 3. Dynamic stability modes of the system.

behavior of the system will exhibit different modes. Fig. (3) shows the plots of the real and imaginary parts of the eigenvalues, λ, which refer to the first and third vibration modes of the system. Dynamic stability (ES) is achieved up to a flow velocity of $v_f = 238.19\,\mathrm{m/s}$. Both modes are coupled with the real parts of, λ, being zero, while their

imaginary parts are non-zero. After this point, these modes become uncoupled. For the first mode, the real part of, λ, is negative, with the imaginary part being zero. In the third mode, the real part of, λ, is zero, and the imaginary part is non-zero. This second dynamic state characterizes divergence instability (DV). From $v_f = 476.38\,\mathrm{m/s}$ to $v_f = 600\,\mathrm{m/s}$, the two modes re-couple, with the real parts of both modes being negative and the imaginary parts non-zero. This third dynamic state characterizes flutter instability (FL).

5 Conclusions

This paper shows that the natural frequencies of the system, without any external point mass added to it, decrease as the fluid flow velocities increase, up to the limit of zero vibration, when the flow velocity reaches the critical value of the system. For higher flow velocities the system presented three different dynamic behaviors. The first, refers to the dynamic stability of the system, where some vibration modes are coupled (the first and third modes, in this case). The second dynamic state is known as divergence, or dynamic instability of divergence. In this case, both vibration modes are non-coupled, up to some flow velocity. The last, is known as dynamic instability of flutter, where the system looses stability, for some value of flow velocity, which is known as the Hopf's bifurcation point. From this point, both modes are re-coupled. As the final observation, already expected for the system, is that with the inclusion of the central mass, its fundamental frequency will, consequently, decrease. However, within the operating limit range, as mentioned before, compared to the free system without the added mass, the rate of change of the natural frequencies is lower. The system tends to be more stable to variations in internal flow velocities, with the addition of an external mass at the middle of the span.

Acknowledgements. "The second author acknowledges support by CNPq (Grant 303529/2021-0), a Brazilian research funding agency."

Authorship statement. The authors hereby confirm that they are the sole liable persons responsible for the authorship of this work, and that all material that has been herein included as part of the present paper is either the property (and authorship) of the authors, or has the permission of the owners to be included here.

References

[1] M. Wu and J. Lou. Effects of rigidity and internal flow on marine riser dynamics. *Applied Ocean Research*, vol. 13, pp. 235–244, 1991.
[2] M. Yamamoto. *A study about the dynamic behavior of flexible tubes including internal flow*. PhD thesis, Yokohama National University, 2011.
[3] M. D. U. Onuoha, Q. Li, and M. Duan. On the interaction between severe slug buildup and dynamic response of a submerged top-tensioned riser. *ASME, 31st International Conference on Ocean, Offshore and Arctic Engineering*, vol. , 2012.
[4] M. Petyt. *Introduction to finite element vibration analysis*. Cambridge University Press, 2nd edition edition, 2010.
[5] S. Timoshenko. *Strength of Materials*. CBS Publishers and Distributors, 1986.
[6] R. D. Blevins. *"Flow-Induced Vibration"*. Krieger, 2nd edition edition, 1994.
[7] R. D. Cook. *"Concepts and applications of finite element analysis"*. Wiley & Sons, 4th edition edition, 2001.
[8] Petrobras. N-57 projeto mecânico de tubulações industriais. vol. , 2017.
[9] I. Grant. Flow-induced vibrations in pipes, a finite element approach. Master's thesis, Cleveland State University, 2001.